Evaluation of the impact of high-resolution winds on the coastal waves

P Sirisha[1],*, P G Remya[1], Anuradha Modi[1], Rabi Ranjan Tripathy[1],
T M Balakrishnan Nair[1] and B Venkateswara Rao[2]

[1]*ESSO-Indian National Centre for Ocean Information Services, Pragathi Nagar, Hyderabad 500 090, India.*
[2]*Institute of Science and Technology, Jawaharlal Nehru Technological University, Hyderabad 500 085, India.*
*Corresponding author. e-mail: sirisha@incois.gov.in

This study discusses the impact of high-resolution winds on the coastal waves and analyses the effectiveness of the high-resolution winds in recreating the fine-scale features along the coastal regions during the pre-monsoon season (March–May). The influence of the diurnal variation of winds on waves is studied for the Tamil Nadu coastal region using wind fields from weather research and forecast (WRF) (3 km) and European Centre for Medium-Range Weather Forecasts (ECMWF) (27.5 km). The improvement in the coastal forecast is then quantified with wave rider buoy observations. The high-resolution wind fields simulated fine-scale features like land–sea breeze events and showed good agreement with observation results. The error in the wave height and period is reduced by 8% and 46%, respectively, with the use of high-resolution forcing winds WRF over ECMWF, although the overestimation of wave energy on high frequencies due to overestimated WRF winds remains as a challenge in forecasting. The analysis also shows the importance of accurate wave forecast during a short-duration sudden wind (~ 12 m/s) occurrence in southern Tamil Nadu near Rameswaram during the pre-monsoon period. Low pressure forms over Tamil Nadu due to the land surface heating, resulting in a sudden increase of winds. High winds and steep waves which cause damage to the property of the coastal community near Rameswaram also were well simulated in the high-resolution forecast system with WRF winds.

Keywords. Wave forecast; wind; sea breeze; wave spectra; maximum wave height; wave steepness.

1. Introduction

Ocean waves play an important role in weather forecasting as they have a direct impact on coastal communities, shipping and marine industry. Extreme ocean waves continue to be a threat to all marine-related activities and hence their accurate prediction is still a topic of research among wave forecasters. Future projection of ocean waves is also of great interest to decision makers with regard to coastal communities, shipping routes and the marine industry (Hemer *et al.* 2013). Timely

information and accurate wave forecast benefit the maritime industry together with millions of coastal populations, who mainly depend on fishing for their livelihood (Schiller *et al.* 2016). Accurate wave forecasting is therefore a primary requirement for the economic growth of countries along coastlines.

Wave forecasting continues to receive considerable attention from both the research and operational communities (Tolman *et al.* 2013). Several countries have already developed and implemented efficient wave forecast systems; European Centre for Medium-Range Weather Forecasts (ECMWF)

(Bidlot *et al.* 2002), National Centre for Environmental prediction (NCEP) (Chawla *et al.* 2013) and Indian National Centre for Ocean Information Services (INCOIS) (Balakrishnan Nair *et al.* 2013) are a few among them. INCOIS is a nodal agency in India that provides the Ocean State Forecast (OSF) for the Indian Ocean (IO) and rim countries. High-resolution wave forecast is a component of INCOIS OSF which uses state-of-the-art wave models like MIKE21 Spectral Wave model (MIKE21 SW), SWAN, WAVEWATCHIII, etc.

The IO holds a unique place among the world oceans due to certain characteristics. A seasonally reversing monsoon wind is a major peculiarity of the IO. Accordingly, the wind climate of the North Indian Ocean (NIO) is categorised as the southwest monsoon (SW, June–September), north-east monsoon (NE, October–January) and pre-monsoon (February–May) (Sabique *et al.* 2012). During the SW monsoon, winds of magnitude of ~ 25 m/s blow from the sea to the land in the SW direction from the Southern Indian Ocean (Das 1995). A complete reversal of the wind is observed during the NE monsoon, i.e., dry surface air blows from the land to the sea in the NE direction (Goswami and Rajagopal 2003). NIO experiences winds (~ 15 m/s) with varying directions during the NE monsoon. After the withdrawal of the NE monsoon, i.e., during the pre-monsoon, winds over the NIO were characterised to be weak in magnitude (<10 m/s) with varying directions. The wind climate is mainly dominated by local winds during this season (Neetu *et al.* 2006; Aboobacker *et al.* 2013).

As the wave climate of NIO comprises three seasons, forecast verification in each season is the most important mainly in managing near-shore activities. Monsoon (SW and NE) season wave characteristics and the reliability of forecasts are addressed in many number of studies (Vethamony *et al.* 2011; Dinesh Kumar *et al.* 2013; Nayak *et al.* 2013; Sirisha *et al.* 2015, 2017; Remya *et al.* 2016; Simpson *et al.* 2002). Among the three seasons, pre-monsoon is generally considered as a season of low-wave activity and hence it has not been given enough attention in the forecast verification so far.

The coastal regions of India experience thermally induced local or mesoscale circulations during summer due to differential heating of the land and ocean surfaces. Land–sea breeze circulation along the coastal regions is one of the best-known examples of such circulation systems that occur at coastal locations of India (Aparna *et al.*

2005; Indira Rani *et al.* 2010). The diurnal variation of winds and its significant impact on the IO and the coastal wave characteristics are already discussed in many studies (Neetu *et al.* 2006; Simpson *et al.* 2007; Aboobacker *et al.* 2011; Glejin *et al.* 2013; Remya and Kumar 2013). In these studies, most of the wave models are forced with coarse-resolution wind fields (spatial resolution of ~ 25 km and temporal resolution of 3 h) for the prediction of coastal waves. But, in reality, these local winds are highly turbulent in nature, exhibiting high spatial and temporal variability (Abdalla and Cavaleri 2002) and hence they cannot be reproduced with coarse resolution (both spatial and temporal) winds. Also, much of the high-frequency nature of winds will not be captured in these coarse winds and this could lead to substantial errors in forecasting the wave fields (Goward Brown *et al.* 2013). In all cases, an accurate coastal wave forecast can be achieved only through the proper representation of the local meteorological events i.e., (land–sea) breezes (Bertotti *et al.* 2013). In the coastal areas where the diurnal variations are prominent, calm sea becomes rough in the afternoon hours due to sea breeze and makes wave forecasting crucial for maintaining the marine activities. There were incidents of boat capsizing during this season near the Indian coastal areas (Vethamony *et al.* 2011).

The objective of the present work is to test the ability of a wave-forecasting system developed for the south-east coast of India to account properly for the most important local effects during the pre-monsoon season with a high-resolution wind. We also try to quantify the improvement in the coastal wave forecast obtained by using high-resolution wind fields of 3 km. In addition to this, a phenomenon of sudden wind rise, locally termed as 'kondalkattu' in the southern Tamil Nadu region during pre-monsoon, is addressed in the final section.

2. Study area

Tamil Nadu is the southernmost state of India bounded by the Bay of Bengal on the east and the IO on the south. Accurate forecasting of waves has a significant role in this region as the coastline constitutes many ports and harbours. ESSO-INCOIS has deployed directional wave rider buoy (DWRB) near Pondicherry (79.86°E, 11.92°N) at a water depth of 15 m as shown in figure 1 and has

been used for validation in this study. Modelling studies were carried out at Tamil Nadu coast during the period March–May 2014.

3. Data and methodology

3.1 *In-situ data*

The wave observations are from DWRB at Pondicherry, which is a part of the ESSO-INCOIS DWRB network around the coastal areas of India. In this study, the observation data from DWRB was used for the assessment of the wave forecasting system (figure 1). The DWRB measures horizontal (roll and pitch) and vertical (heave) accelerations using two accelerometers and an onboard compass which gives directional displacements in two horizontal axes. The displacements are converted to wave parameters using in-built software in the buoy. The DWRB measures waves with periods in the range of 1.6–30 s, and heave motion in the range of −20 to +20 m with a resolution of 1 cm. Wave direction measurement was obtained in the range of 0°–360° with a directional resolution of 1.5° and an accuracy of 0.5° with reference to the magnetic north. The buoy data records were taken at a frequency of 1.28 Hz for 17 min every half an hour. The quality check of the measured time series data was conducted for standard errors such as spikes, steepness and constant signals (Barstow and Kollstad 1991). The buoy-wave spectra were obtained using fast Fourier transforms. Different wave parameters like significant wave height (H_s), maximum wave height (H_{max}), peak-wave period (T_p) and peak-wave direction (P_{dir}) were derived from the wave spectrum. The real-time data were received from INCOIS through the Indian National Satellite System (INSAT)/Global System for mobile communication (GSM) modes. H_s is the average of one-third of the highest waves. H_{max} is the maximum wave height during a record. T_p (in seconds) is defined as the wave period associated with the most energetic waves in the total wave spectrum at a specific frequency. P_{dir} is the direction associated with the highest-energetic wave in the total wave spectrum. Significant wave steepness of the wave parameter from the buoy is computed by dividing the significant wave height (H_s) with the wavelength (L_s) of the wave shown in equation (1).

$$\xi(f) = \frac{H_s(f)}{L_s(f)} = \frac{2\prod H_s(f)}{gT_z(f)^2} \tag{1}$$
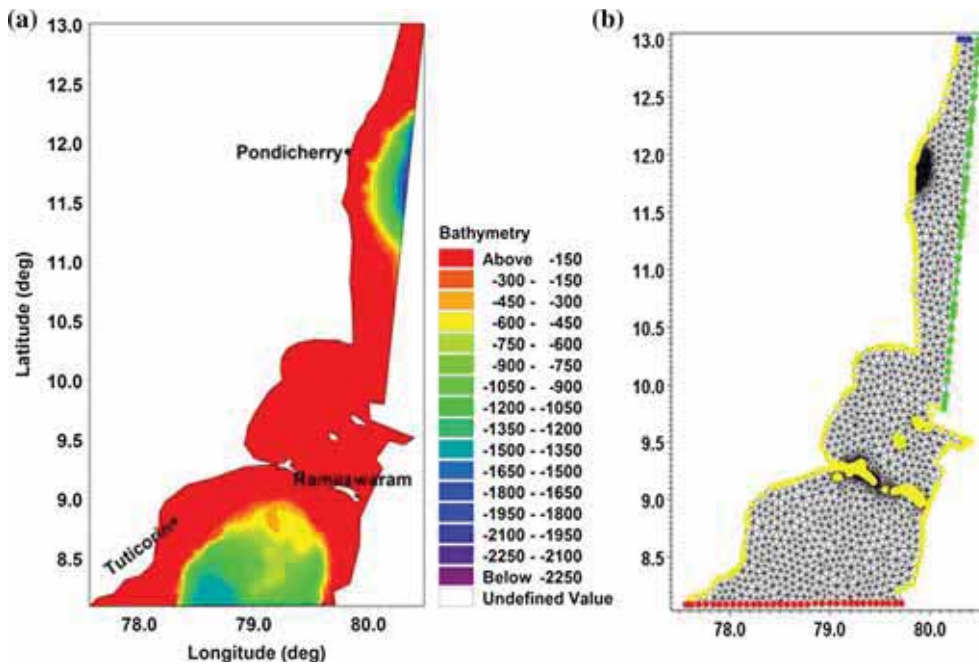
$$H_s(f) = 4\sqrt{m_o} \tag{2}$$

Figure 1. The plot (**a**) shows the model domain and bathymetry. The observations used in the study are marked with black circles. Plot (**b**) shows a fine-resolution mesh used in the model domain. The boundaries of the domain marked with yellow represents the land and red, green and blue colors are represents the ocean boundary.

$$T_z(f) = \sqrt{\frac{m_o(f)}{m_2(f)}} \qquad (3)$$

$$m_n(f) = \int_{f_l}^{f_u} f^n S(f)\, df \qquad (4)$$

Where H_s and T_z are given in equations (2 and 3). Here $\xi(f)$ corresponds to the wave steepness parameter at all frequencies f: H_s is the significant wave height of the wave associated with wavelength (L_s) and the average wave period (T_z). Equation (4) shows the parameters corresponding to the nth moment of the wave spectrum. In this work, we have used integral wave parameters such as H_s, T_p and P_{dir} from the buoy to assess the model performance during the period Mar–May 2014. We analysed parameters like wave steepness and H_{max} from observation and a model to understand the localised phenomena prevailed near the coastal areas during the pre-monsoon season.

As a part of the study, we made the assessment of winds using Advanced SCATterometer (ASCAT) observations at this location. ASCAT represents the latest implementation of spaceborne microwave wind measuring scatterometry (Bentamy and Fillon 2012). ASCAT wind products are processed by NOAA/NESDIS utilising measurements from a scatterometer instrument on board the EUMETSAT Metop Satellites. The instrument uses a radar to measure the backscatter and further determine the speed and direction of winds over the surface of the oceans. Surface wind images are created for ascending and descending (25 × 25) km resolution data.

3.2 *Automated weather station (AWS)*

An AWS which measures the metrological parameters such as wind speed and direction, air temperature, relative humidity and pressure were installed by the INCOIS and IMD near the coastal areas. The accuracy of the wind speed is 0.2 m/s in the range of 0–60 m/s and the accuracy of the wind direction is 3°. The AWS set at a height of 3 m near the coastal areas in Tuticorin (78.2°E, 8.8°N), Gopalpur (84.96°E, 19.31°N), Paradip (86.65°E, 20.26°N), Ratnagiri (73.28°E, 16.89°N) and Karwar (74.13°E, 14.85°N) coastal stations. The observed wind speeds from the AWS were used to evaluate the forecast winds at the respective coastal locations during the period March–May

2014. The observed wind data from the AWS were useful in the qualitative comparison of forcing winds near the coastal locations.

Peixoto and Oort (1992) suggested an empirical logarithmic profile which converts observed winds from AWS at a height of 3–10 m. If the wind speed at 3 and 10 m is represented as Ws (3 m) and Ws (10 m), respectively, then the winds at 3 m are converted to 10 m by using equation (5). Here $Z = 10$ m, $Z_{ref} = 3$ m and $Z_0 = 1.52 \times 10$ (Indira Rani and Das Gupta 2013)

$$Ws(10m) = Ws(3m)\frac{\ln\left(\frac{Z}{Z_0}\right)}{\ln\left(\frac{Z_{ref}}{Z_0}\right)} \qquad (5)$$

3.3 *Forcing fields*

Wave-model simulations greatly depend on the quality of the forcing fields (Cavaleri 1994) and hence fine-resolution forcing winds are essential for an accurate prediction of the wave parameters. In this study, we have simulated the SW model under two different forcing winds; winds from the WRF model and the ECMWF model for the period March–May 2014. More details of the wind fields are given below.

3.3.1 *WRF wind fields*

The WRF model is a mesoscale numerical weather prediction (NWP) system designed for both atmospheric research and operational forecasting applications (Michalakes *et al.* 2004; Powers *et al.* 2017). A high-resolution mesoscale numerical model WRF-ARW-3.7 (Skamarock *et al.* 2008) was configured and set up at ESSO-INCOIS for operational forecasting. The ESSO-INCOIS WRF model provides atmospheric forecast winds for 72 h with a high spatial (3 km) and temporal (1 h) resolution for the domain range (0–25°N, 65–95°E) which uses initial and boundary conditions from the Global Forecast System of the National Centre for Environmental Prediction. The WRF model winds predict the diurnal variability (land–sea breeze cycle) of the surface wind in the coastal region realistically (Vishnu and Francis 2014).

3.3.2 *ECMWF wind fields*

ECMWF uses the NWP technique to forecast weather from its present measured state. This

takes account of input from the meteorological data, collected by satellites and earth observation systems such as automatic and manned stations, aircraft, ships and weather balloons. All data fed into ECMWF's databases are assimilated into the NWP models. The output products from these models are the medium-range forecasts that predict the weather up to 15 days ahead (Andersson 2013). The spatial and temporal resolution of the forecast winds are of 27.5 km and 3 h interval, respectively.

3.4 *Numerical wave model*

MIKE 21 SW is the state-of-the-art third-generation spectral wind-wave model based on unstructured meshes which was developed by the Danish Hydraulic Institute (DHI), Denmark. The model simulates the growth, decay and transformation of wind-generated waves and swells in the offshore and coastal areas. MIKE 21 SW is particularly applicable for simultaneous wave prediction and analysis on a regional and local scale. The SW model includes the following physical phenomena: (i) Wave growth by the action of wind, (ii) nonlinear wave–wave interaction, (iii) dissipation due to white capping, (iv) dissipation due to bottom friction, (v) dissipation due to depth-induced wave breaking, (vi) refraction and shoaling due to depth variations, (vii) wave–current interaction and (viii) the effect of time-varying water depth. All source terms and equations related to the model are explained in detail in Sorensen *et al.* (2004).

The SW model is based on a flexible mesh and is therefore suitable for both regional- and local-scale wave modelling allowing for a fine-resolution mesh in shallow regions and a coarse-resolution mesh in the offshore regions. The use of an unstructured mesh enhances the accuracy of the wave model near complex areas of the coastline. The model solves the wave action balance equation; spatial discretisation is performed using an unstructured finite volume method. The integration in time is based on a fractional-step approach, where the propagation steps are solved using an explicit method (DHI 2014). The SW model was implemented and validated for several regions (Golshani *et al.* 2005; Jose *et al.* 2007). Many researchers used SW for describing the wind and wave climate in the IO region (Vethamony *et al.* 2006, 2009, 2011; Aboobacker *et al.* 2009, 2011, 2013, 2014; Kurian *et al.* 2009; Remya *et al.* 2012; Sabique *et al.* 2012).

All these studies show the SW model performs well for the IO region.

This section discusses about the high-resolution coastal model domain for the Tamil Nadu region as shown in figure 1. The model domain extends from 77.5–80.5°E to 7–13°N, preferably showing the near-shore bathymetry almost the entire region. Mesh resolution varies from 1 km (near the coast) to 10 km (offshore). The required boundary conditions for the coastal model domain are taken from a regional IO model domain (30–120°E; 30°N–60°S). The resolution of the regional model varies from 15 km (near the coast) to 100 km (offshore). Wave forecast verification of the regional setup during normal seasons and extreme wave conditions are already described in the studies by Balakrishnan Nair *et al.* (2013) and Sirisha *et al.* (2015). Modified Etopo2 bathymetry data were used for the bottom effects. Modified Etopo2 contains improved shelf bathymetry for the IO region (20–112°E and 38°S to 32°N) which is derived by digitising the depth contours and sounding depths less than 200 m from the hydrographic charts published by the National Hydrographic Office, India (Sindhu *et al.* 2007). The present model setup uses a spectral resolution of 28 frequencies and 24 directions. The SW model was simulated during the period March–May, 2014 using WRF and ECMWF winds as forcing fields. Output wave parameters from the simulation like significant wave height, peak-wave period and peak-wave direction and spectral parameters at the Pondicherry location are saved at 3 h intervals for the respective wind fields.

3.5 *Methodology*

Forecasted-wave parameters from the SW model were assessed quantitatively using several statistical measures such as bias, root mean square error (RMSE), scatter index (SI) and correlation coefficient (R). Bias, the mean difference between the model and observation, indicates average overestimation (positive) or underestimation (negative) of forecast compared to observation. The root mean square error is a frequently used statistical parameter to measure the differences between forecast and observation values. RMSE serves to aggregate the magnitudes of the errors in the forecast. The SI is another important statistical parameter to describe the forecast error. It is defined as the standard deviation of the difference between the model

output and observation, normalised by the mean of observation. Lower values of SI indicate better model performance. The Pearson correlation coefcient is a measure of the degree of linear dependence between the model and observation. The correlation values range from −1 to +1. A value of high-positive correlation signifies to what extent the forecast data follow the trend of observation (Steven *et al.* 2016; Bryant *et al.* 2016; Sirisha *et al.* 2017). The formulas of the above-listed statistical parameters are given in equations (6–9)

$$\text{Bias} = \sum_{i=1}^{N} \frac{1}{n} (M_i - B_i) \qquad (6)$$

$$\text{RMSE} = \frac{1}{n} \sqrt{\sum_{i=1}^{N} (M_i - B_i)^2} \qquad (7)$$

$$\text{SI} = \frac{\text{RMSE}}{\bar{B}} \qquad (8)$$

$$R = \frac{\sum (M_i - \bar{M}) (B_i - \bar{B})}{\sqrt{\sum_{i=1}^{N} (B_i - \bar{B})^2} \sqrt{\sum_{i=1}^{N} (M_i - \bar{M})^2}} \qquad (9)$$

Here B_i and M_i refer to the buoy measured and forecasted-wave parameters, respectively, $\bar{B}$ and $\bar{M}$ are the mean values and n is the number of observations used for comparison.

4. Results and discussion

4.1 *Diurnal variations of wind and wave at Pondicherry*

Initially an assessment of the forecast winds, both WRF and ECMWF, in the coastal regions is carried out using available coastal-AWS observations. Figure 2 shows a comparison of forecasted winds with observed winds (AWS) at four locations, Gopalpur, Paradip, Karwar and Ratnagiri, during the period April 21–30 2014.

During the representative period, observed wind speed shows calm winds (2–10 m/s) near the east coast and (1–6 m/s) near the west coast with a clear diurnal cycle on both coasts. Most of the time, WRF winds are in good agreement with the observed winds at Gopalpur and Paradip. But ECMWF shows consistent peaks for the wind speed (>5 m/s) at these coasts. Observed wind directions varied preferably (N–NE) during this

period. Both WRF and ECMWF showed a reasonable agreement in the case of wind directions with observation (figure 2a and b). Wind speeds from observation near the west coast (figure 2c and d) were comparatively low (<5 m/s) than the east coast (figure 2a and b) during this period. It is interesting to note that there was a sudden rise in observed wind speed of ∼10 m/s near Karwar on 28 April 2100 UTC which was forecasted by WRF and missed by ECMWF. The rapid variations of wind directions in the observation were reasonably agreed for both forecast winds near the Karwar and Ratnagiri coasts.

Quantitative assessment of the forecast winds with observation during the pre-monsoon season was carried out at these four locations and the error statistics is shown in table 1. Positive bias seen in both WRF and ECMWF shows overestimation in the forecasts during this season. RMSE values of WRF were lesser (1.04–1.54 m/s) than those of ECMWF (1.38–2.80 m/s). Also, the SI values displayed in table 1 show low values for WRF (27–38%) and high values for ECMWF (42–64%) during the study period. *R* values were found to be high for WRF (0.73–0.88) and low for ECMWF (0.37–0.66). The low values of SI along with high *R*, obtained for WRF winds confirm a good linear agreement over ECMWF during the study period. The statistics strongly support the WRF high-resolution winds during the pre-monsoon season.

A comparison of wind and wave parameters at Pondicherry is displayed in figure 3. As AWS winds are not available at Pondicherry, the comparison was carried out with ASCAT winds. The quality of the ASCAT wind fields in the northern IO is determined in the study of Sivareddy *et al.* (2015). Assuming that ASCAT winds were accurate, a comparison was made between the forecast (WRF and ECMWF) and ASCAT wind fields as shown in figure 3(a). From the scatter plot (figure 3a), it is clear that both observed and forecast winds were predominantly weak (<10 m/s) during this period at Pondicherry. The overall comparison and statistics present in table 2 signies the good agreement of WRF (SI = 19%, *R* = 0.77) forecast winds with ASCAT compared to ECMWF (SI = 33%, *R* = 0.60) (table 2).

The sensitivity of the wave model to the differences in the wind fields is determined by the comparison of H_s, T_p and P_{dir} with observations (figure 3b–d). During the pre-monsoon season, both observed and forecasted-wave heights were in the range of 1–1.5 m near the Pondicherry coast.
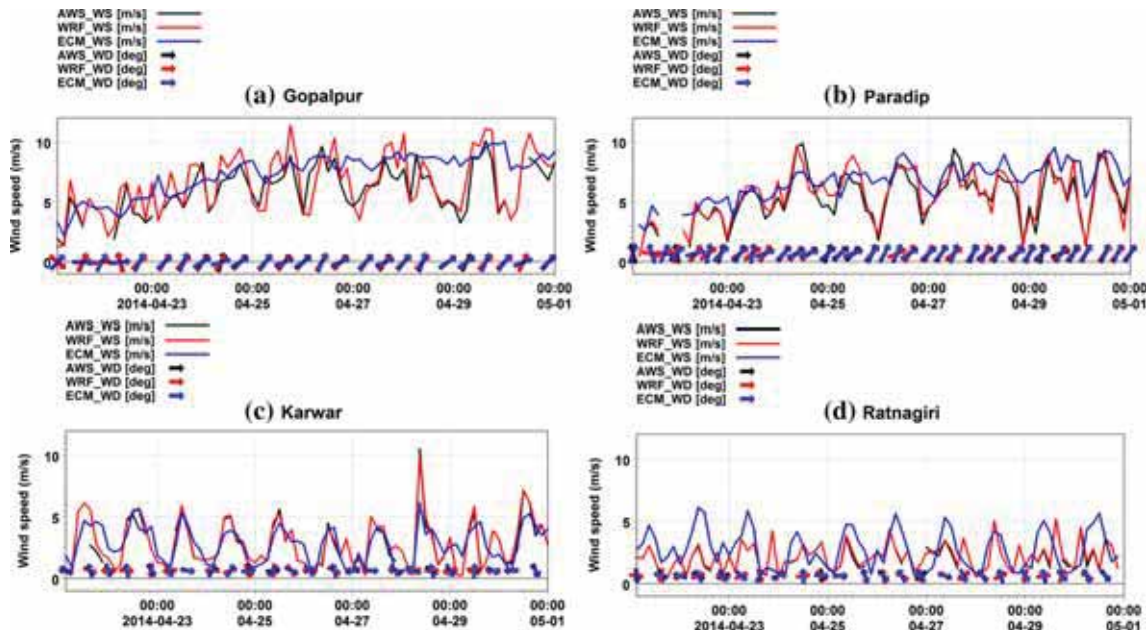
Figure 2. Time series plot of AWS observed and forecasted (WRF and ECMWF) wind speeds near the coastal areas of India.

Table 1. *Error statistics computed between forecasted and observed wind speeds in coastal areas of India.*

Coastal locations	Forecast winds	Bias (m/s)	RMSE (m/s)	SI (%)	R	N
Gopalpur	WRF	0.69	1.54	27	0.83	502
	ECMWF	1.56	2.42	43	0.56	502
Paradip	WRF	0.95	1.47	34	0.88	656
	ECMWF	2.20	2.80	64	0.66	656
Karwar	WRF	0.71	1.06	32	0.83	729
	ECMWF	0.66	1.38	42	0.56	729
Ratnagiri	WRF	1.03	1.04	38	0.77	731
	ECMWF	1.52	1.59	58	0.37	731

Simulated H_s from both ECMWF and WRF was comparable to the observation results. Statistics shows a better performance of WRF with a low SI (=22%) and high R (=0.71) compared to ECMWF (figure 3b and table 2). The peak period and direction from observation shows (4–15 s) waves from the north-east–south-east (45°–180°) at the location indicating a mixed sea state (figure 3c and d). It can be clearly noticed that high-resolution WRF winds reasonably reproduced the low-wave periods, i.e., wind sea in the observation whereas ECMWF exhibited high deviation from the observation. Hence, the error statistics of ECMWF exhibited large deviation in T_p (SI$_{ECMWF}$ = 81%).

The time evolution of the observed wave parameters during the pre-monsoon period is shown in figure 4. During the study period, H_s ranges from 0.2 to 1.5 m and T_m (mean period) from 4 to 10 s (figure 4a–c). The diurnal variations are clearly noticed in the time evolution of the wave field. Observed H_s showed an increase of wave height from 0900 to 1500 UTC and a decrease afterwards (figure 4a–c). This indicates the growth of wind waves during the sea breeze period (0900–1500 UTC). It is interesting to note that a marked increase in wave height can be seen in the observation whereas variations in the T_m were not clearly seen unlike other coastal areas of India. For instance, it is well known that the swell-dominated sea state changes to a sea-dominated state near the coastal areas of Ratnagiri and Goa. The sudden change of the sea state is manifested by a marked decrease of the wave period in a mixed sea-state during the sea-breeze period (Neetu *et al.* 2006; Aboobacker *et al.* 2013). South-east coastal areas are mostly wind sea dominated due to the sheltering effect of Sri Lanka (Anoop *et al.* 2015), and hence during the sea breeze period, the dominant
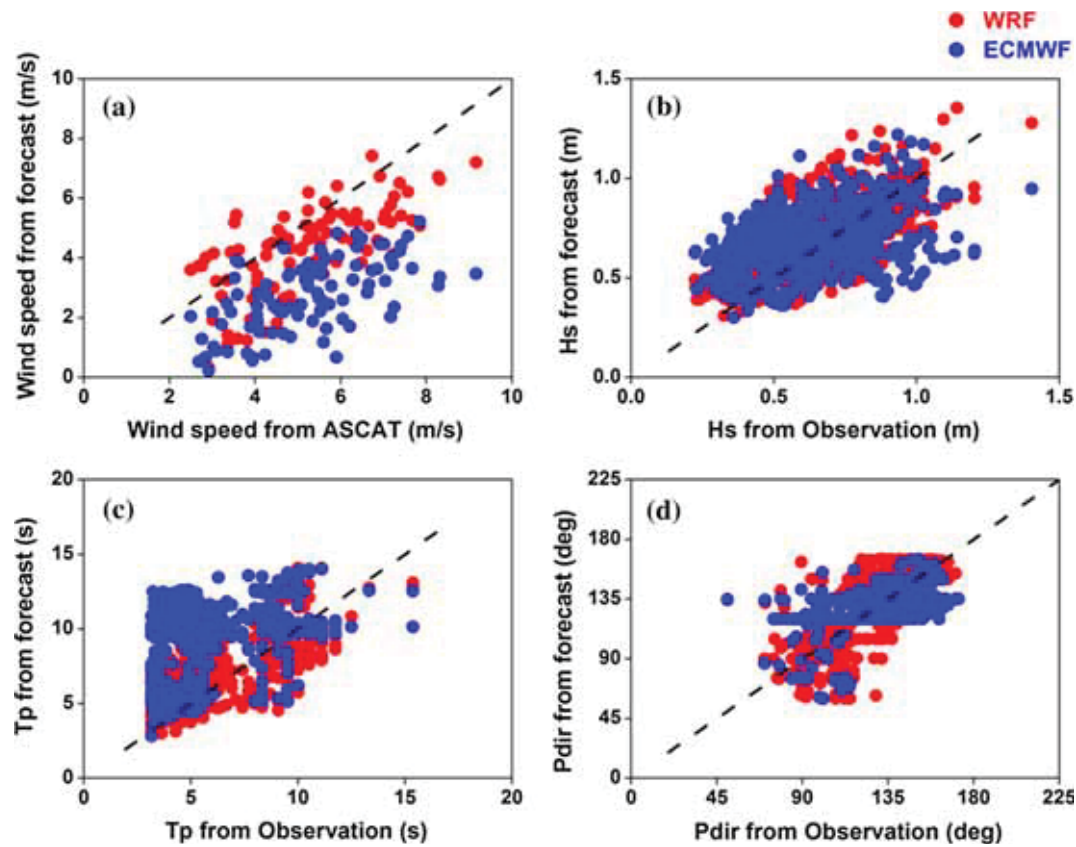
Figure 3. Scatter plot of wind and wave parameters at Pondicherry. Plot (**a**) shows a comparison of forecast winds with ASCAT. Plots (**b–d**) show a comparison of forecasted H_s, T_p and P_{dir} with observation, respectively. The identity line is represented by dashes in all the plots.

Table 2. *Error statistics computed between forecasted and measured wave parameters at Pondicherry.*

Statistics	Simulations	Bias	RMSE	SI (%)	R
Wind speed (m/s)	WRF	0.24	1.00	19	0.77
	ECMWF	−1.25	1.74	33	0.60
H_s (m)	WRF	0.03	0.14	22	0.71
	ECMWF	0.04	0.19	30	0.43
T_p (s)	WRF	0.91	2.05	35	0.70
	ECMWF	3.76	4.68	81	0.31
P_{dir} (°)	WRF	0.31	19.42	15	0.68
	ECMWF	−1.03	18.72	14	0.54

frequency shift occurs in the higher frequency part itself, for instance, period changes from 6 to 5 s.

Furthermore, we have made an attempt to study the spectral energy density in the frequency–time domain to assess the impact of high-resolution forcing winds on wave. The bulk wave parameters do not change significantly until there is a large variation in the wave spectrum (Sanil Kumar and Anjali Nair 2015) and hence a study of the wave spectrum in the frequency–time domain is

important to identify the characteristics of spectral changes during sea breeze. Time evolution of observed and forecast-spectral energy density in the frequency domain for the study period is shown in figure 5.

In March, the observed-wave spectra showed multi peaks mainly in the high-frequency region. The magnitude of the energy density in the observation was varied up to 1 m²/Hz and the energy was confined to the frequency range of
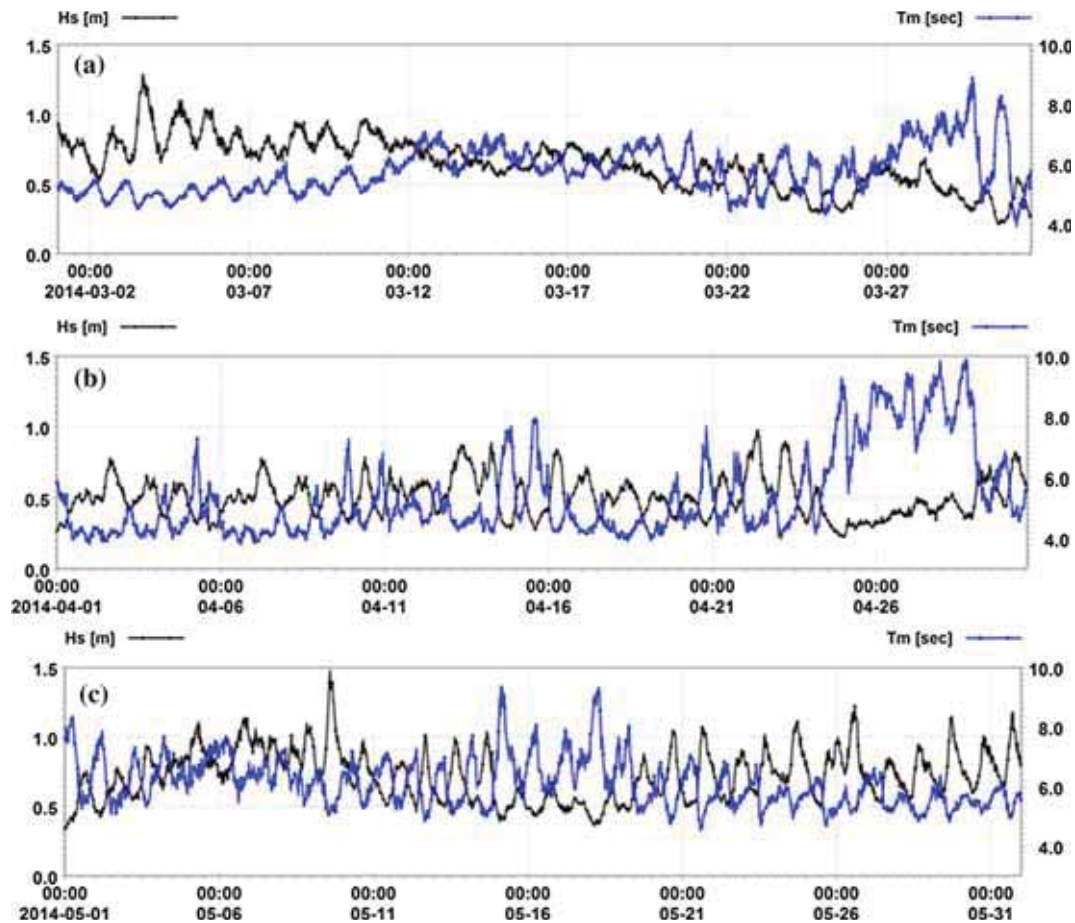
Figure 4. Time series plots of H_s and T_m from observation at Pondicherry during the months of (**a**) March, (**b**) April and (**c**) May, respectively.

0.1–0.4 Hz (figure 5a). Peak frequencies (PF) were mainly concentrated around 0.2 Hz which show the domination of local wind seas in Pondicherry during this month. The spectrum was void of low frequencies most of the times during this month. In the case of WRF (figure 5b), the spectral energy spread over the frequencies of 0.1–0.4 Hz with a dominant peak around 0.2 Hz as seen from observation (figure 5a). The magnitude of energy density varied in the range of 0–2 m^2/Hz in WRF (figure 5b) which indicates an overestimation compared to observation. But high-spatial and temporal resolution of WRF winds well reproduced the spectral energy distribution clearly over high frequencies similar to that of the one from observation. Along with high frequencies, WRF spectra had a low-frequency component also. ECMWF wind fields had generated spectra over the frequency region (0.1–0.25 Hz; figure 5c), but most of the time, the energy distributed over the low-frequency region and model failed in reproducing peaks in the high-frequency region (PF > 0.2 Hz) as shown in the observation.

During the month of April, it was noticed that the observed wave spectra (figure 5a) showed dominant peaks near the frequency 0.3 Hz. The magnitude of spectral energy (0–1 m^2/Hz) spread over the frequencies of 0.1–0.4 Hz and observation shows dominant peaks over the high-frequency region throughout this month that indicates the domination of wind seas. It is interested to note that the swells are also dominant during some of the days (20–30 April). The spectrum exhibits the characteristic nature of multi peaks at higher frequencies mostly and double peaked spectra occasionally during this month. The wave spectrum from WRF shows the dominant peaks over the high-frequency region as that of observation around the PF of 0.2–0.3 Hz (figure 5b). The magnitude of the energy density varied in the order of 0–2 m^2/Hz (figure 5b) near the spectral peak. The spectrum shows the distribution of spectral energy over wide frequencies from 0.1 to 0.35 Hz, which points out the existence of a primary peak on lower frequencies and a secondary peak on high frequencies. As mentioned earlier,
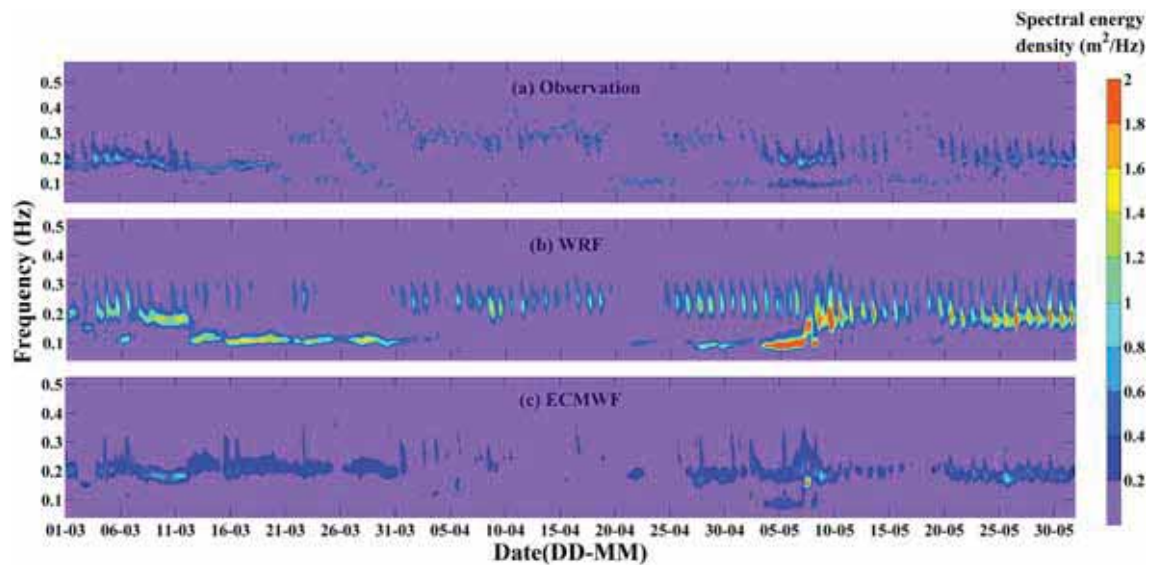
Figure 5. Contour plots of spectral energy density in frequency–time domain at Pondicherry (**a**) observation, (**b**) WRF and (**c**) ECMWF during the months of March, April and May.

ECMWF missed the peaks in the high-frequency region (figure 5c).

During the month of May, the buoy spectrum (figure 5a) showed a characteristic feature of double peaks throughout the period with a dominant primary peak with a higher frequency and a secondary peak with low frequencies. The spectral energies (~ 1 m^2/Hz) distributed over the frequency range of 0.1–0.4 Hz. Figure 5(b) shows that the WRF forecast spectrum has the distribution of spectral energies over the frequency range of 0.05–0.35 Hz. Further wave spectrum (WRF) accurately reproduced the energy variations on low- and high-frequency regions as that of observation and confirmed the presence of a double-peaked spectrum throughout this month. The magnitude of energy densities are varied up to 2 m^2/Hz in the model and overestimated in the high-frequency peak. The overestimation of energy density in the WRF spectrum in the high-frequency region could be from the overestimation of WRF winds during the study period. The high-frequency peaks from observation were not properly simulated by the ECMWF wind fields here as well (figure 5c).

A detailed analysis of the spectral characteristics of the waves during land–sea breeze periods has been performed for randomly chosen representative days in each month as shown in figure 6. The analysis helps in understanding the importance of high-resolution wind fields in simulating the local features or high-frequency variations in the wave

model. The spatial and temporal variations of WRF wind were very high (3 km and hourly), which plays a crucial role in picking variations over high-frequency regions. Figure 6 shows the normalised energy spectrum for both observation and model simulation. From figure 6(a–d), the characteristic feature of broad spectra which have multiple peaks (0.1–0.5 Hz) over the high-frequency region in March can be observed. The spectra from WRF show two peaks (PF < 0.1 Hz and PF > 0.2 Hz), and overall, a reasonable match between the observed and forecasted (WRF) spectrum is noticed. The forecasted spectrum (ECMWF) shows a dominant peak at PF <0.1 Hz and none of the high-frequency peaks are reproduced by the forecast, which strongly suggests that the model is unable to simulate the local wind seas during this month. In April, figure 6(e–h) shows that observation has a small peak at ~ 0.1 Hz and a dominant peak at ~ 0.3 Hz suggesting a characteristic bimodal spectrum during this month. The model forecasted spectrum (WRF) shows two peaks corresponding to PF ~ 0.1 and 0.3 Hz, suggesting a good match between forecast and observation whereas the ECMWF forecasted spectrum has not shown any peak in the high-frequency region. In May, the observed spectrum has shown two dominant peaks corresponding to 0.1 and 0.2 Hz, i.e., towards the low- and high-frequency regions (figure 6i–l). A good match found between the forecasted spectra (WRF) and observation during this month. However, the ECMWF forecasted
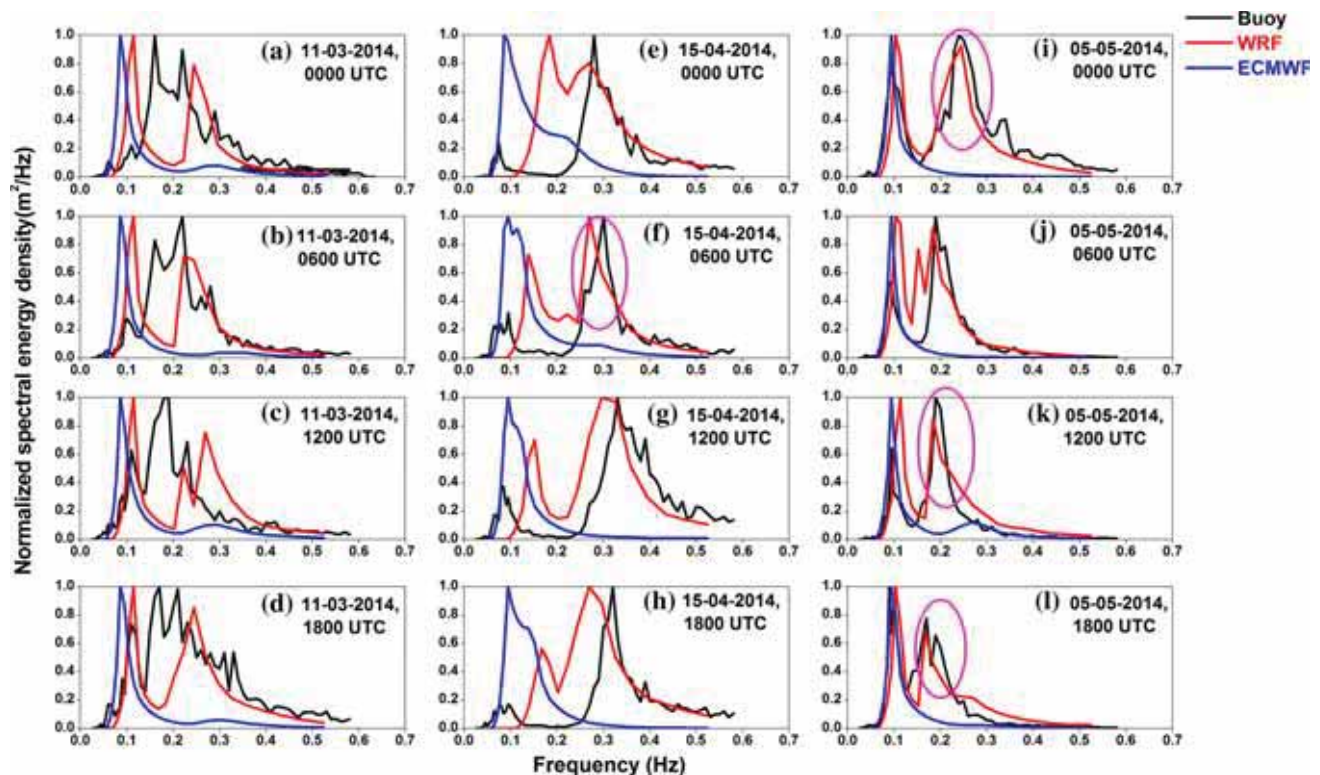
Figure 6. Comparison of frequency–energy wave spectra from (WRF & ECMWF) simulation with observation. The circles marked with pink colour shows good match of WRF spectrum with observation.

spectrum (ECMWF) did not show any peaks in the high-frequency region. Figure 6 clearly shows that most of time, the WRF wave spectral shapes were in good agreement with those from observation (marked with circles in figure 6).

WRF wind (3 km and 1 h) spatial and temporal resolutions reasonably reproduced the high-frequency variations as that of the observation spectrum. The spatial and temporal resolution of the ECMWF winds were not adequate for reproducing the local features and could not generate high-frequency variations as observed and the spectrum was mostly single-peaked in a low-frequency region throughout the day which causes false alarms in the forecast.

The overall study suggests the good match obtained with a forecasted spectrum with WRF and a poor match is seen in the case of the ECMWF spectra especially in the simulating peaks of the high-frequency region. However, the magnitudes of energy densities near the spectral peaks were overestimated by WRF and that resulted in the overestimation of H_s during the pre-monsoon season. Despite an overestimation, the error statistics was found to be in the accepted range for operational use (Woodcock and Greenslade 2007).
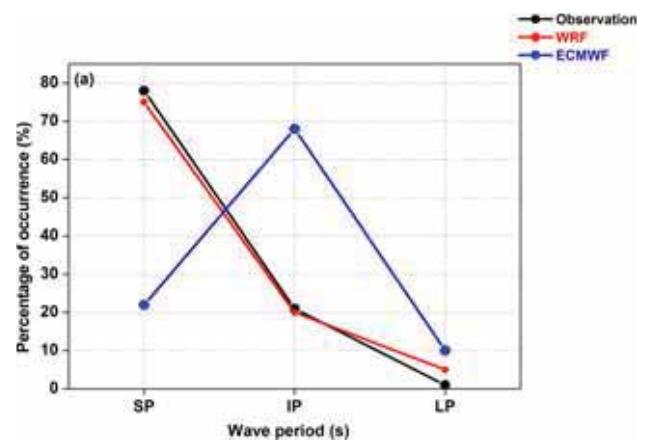

Figure 7. Percentage of occurrence of wave periods at Pondicherry.

To identify the dominant wave periods during this season, we have made a comparison of the percentage of occurrence of short period (SP) (<8 s), intermediate period (IP) (8–12 s) and long period (LP) (>12 s) waves from observation and simulations at Pondicherry (figure 7). During the pre-monsoon season, both observation and WRF show that 80% of the time, the coast experiences

SP waves and 20% of the time, IP waves and 10% of time, LP waves. The ECMWF forecast shows the percentage of occurrence of IP waves which are more than that of the SP and LP waves. Overall analysis shows that the Pondicherry coast experiences SP waves with PF in the range of 0.2–0.3 Hz, indicating dominant wind seas during the pre-monsoon season.

4.2 *Impact of short-duration strong winds on waves*

During the pre-monsoon season, short-lived high wind occurrences are noticed near the areas of the Rameswaram region of southern Tamil Nadu. These winds are locally known as kondalkattu (termed by fisherfolk) which is not yet addressed in any scientific literature. Accurate wave forecasts during such events are also very important in the study area as it affects the coastal community. Initially, we provided a comparison of wind and analysed the reason for the occurrence of a short duration strong winds. Due to the unavailability of the observed wind data at Rameswaram during the study period, we

considered the AWS wind data of Tuticorin (figure 1) for establishing the reliability of forecast winds (figure 8a and b). It is clear from figure 8(a) that the location is predominated by weak winds (<10 m/s) during the study period. The statistics are displayed in table 3. Error statistics suggests that WRF (SI = 32%, $R = 0.74$) winds were in good agreement with observation compared to ECMWF (SI = 44%, $R = 0.67$). It can be clearly noticed that SI has increased by 12% in the ECMWF forecast compared to WRF. The wind directions of the WRF forecast were able to reproduce the observed wind directions and exhibited high correlation with observation than that of ECMWF.

In general, the winds near Rameswaram are weak (~ 10 m/s) during the pre-monsoon season but a sudden increase in the wind speed was noticed for a few days (2nd, 4th and 5th May 2014) as shown in figure 8c and d. An increase in the wind speed was noticed only in the WRF forecast but not in ECMWF. An analysis of the WRF wind fields shows that a patch of high winds developed in the area of Rameswaram and dissipated within three hours during the kondalkattu days. The
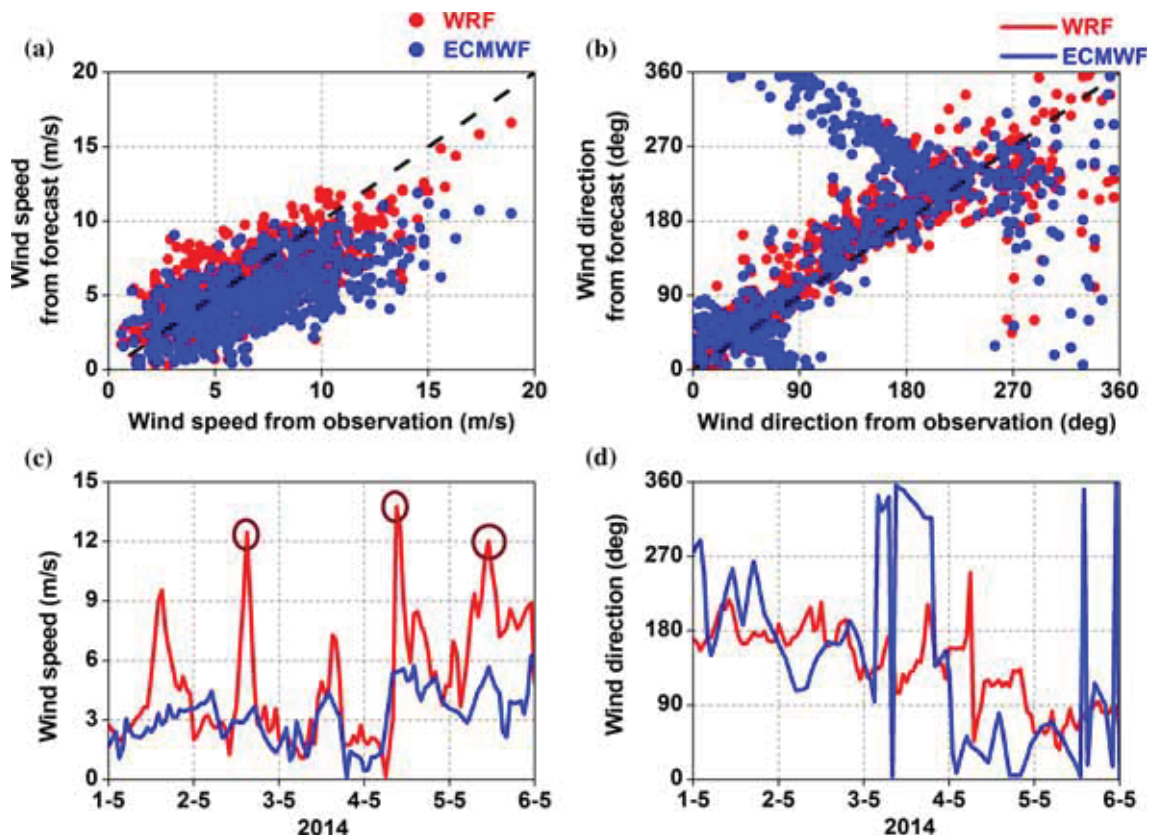

Figure 8. Plots (**a** and **b**) refer to a comparison of forecast wind speeds and wind directions with observation at Tuticorin. Plots (**c** and **d**) show the time series plot of WRF and ECMWF wind speed and directions at Rameswaram from 1–6 May 2014. A sudden increase in wind speed events is marked with circle.

Table 3. *Error statistics computed between forecasted and measured wave parameters at Tuticorin.*

		Bias (m/s)	RMSE (m/s)	SI (%)	R (N = 647)
Wind speed (m/s)	WRF	−0.63	2.22	32	0.74
	ECMWF	−1.90	3.01	44	0.67
Wind direction (°)	WRF	10.16	41.56	30	0.88
	ECMWF	21.44	84.79	61	0.61

Figure 9. Plots (**a** and **b**) show forecasted sea-level pressure and wind speed from WRF at 1500 UTC on 2 May 2014, respectively. Plot (**c**) shows the ascending path of ASCAT observation winds near Rameswaram on 2 May 2014.

coarse resolution of ECMWF winds completely missed this feature. To understand the increase in wind speed during these days, we have selected one of the short duration strong wind events, i.e., on 2 May 2014. Figure 9(a) shows the formation of high pressure over Sri Lanka and low pressure over Tamil Nadu (Salem; 78.14 E, 11.66 N) on 2 May 2014. High wind blows because of the difference in pressure, i.e. from a high to low pressure area (figure 9b). The sustenance of a low-pressure system over Salem was short (<3 h) from 1400 to 16,000 UTC on 2 May 2014, and hence high winds

also sustained for a SP. A satellite observation from the ASCAT path near Rameswaram has shown high winds (∼12.86 m/s) on 2 May 2014 (figure 9c). It is interesting to note that the wind direction has not shown any remarkable change during this period. Analysis of other events also supports the fact that, in April and May, the variation in land surface cooling induces a low pressure centred around Salem (Tamil Nadu, 11.65°N, 78.16°E) and this causes the sudden intensification of winds in the area between Salem and Sri Lanka marked in figure 9(a and b). ESSO-
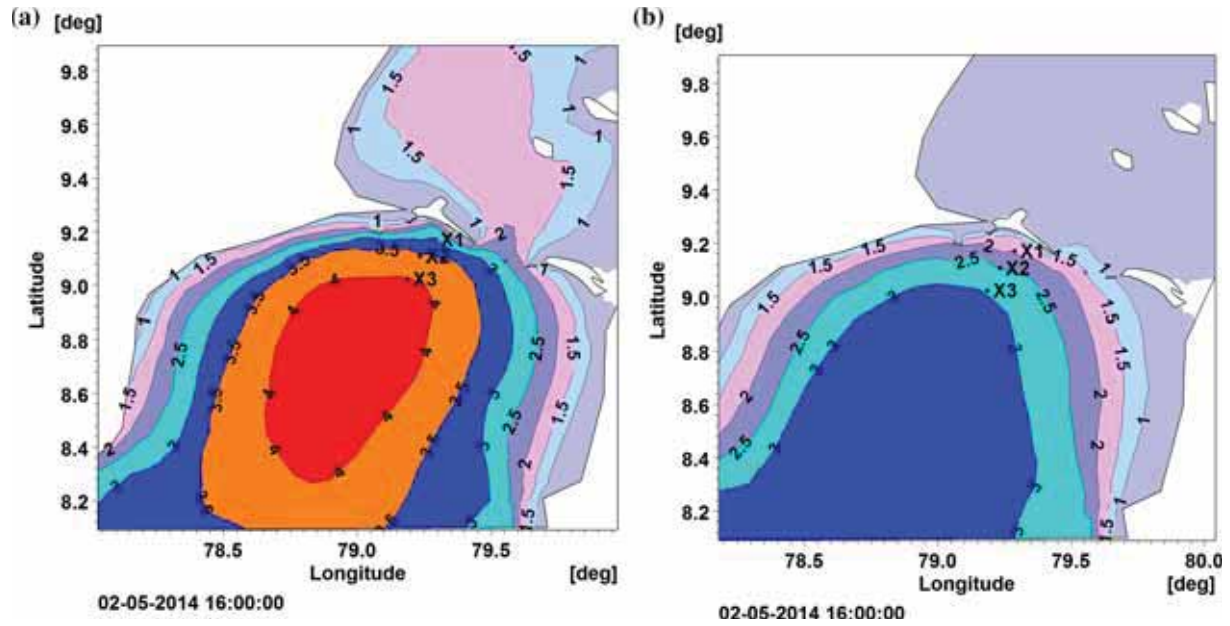
Figure 10. Propagation of the highest energetic wave (H_{max}) at Rameswaram during one of the kondalkattu events. Plots (**a** and **b**) refer to H_{max} obtained from the simulations with forcings (WRF, ECMWF), respectively. The points located (X1, X2 and X3) are at a distance of (8, 17, 28) km away from the southern end of Rameswaram coast, respectively.
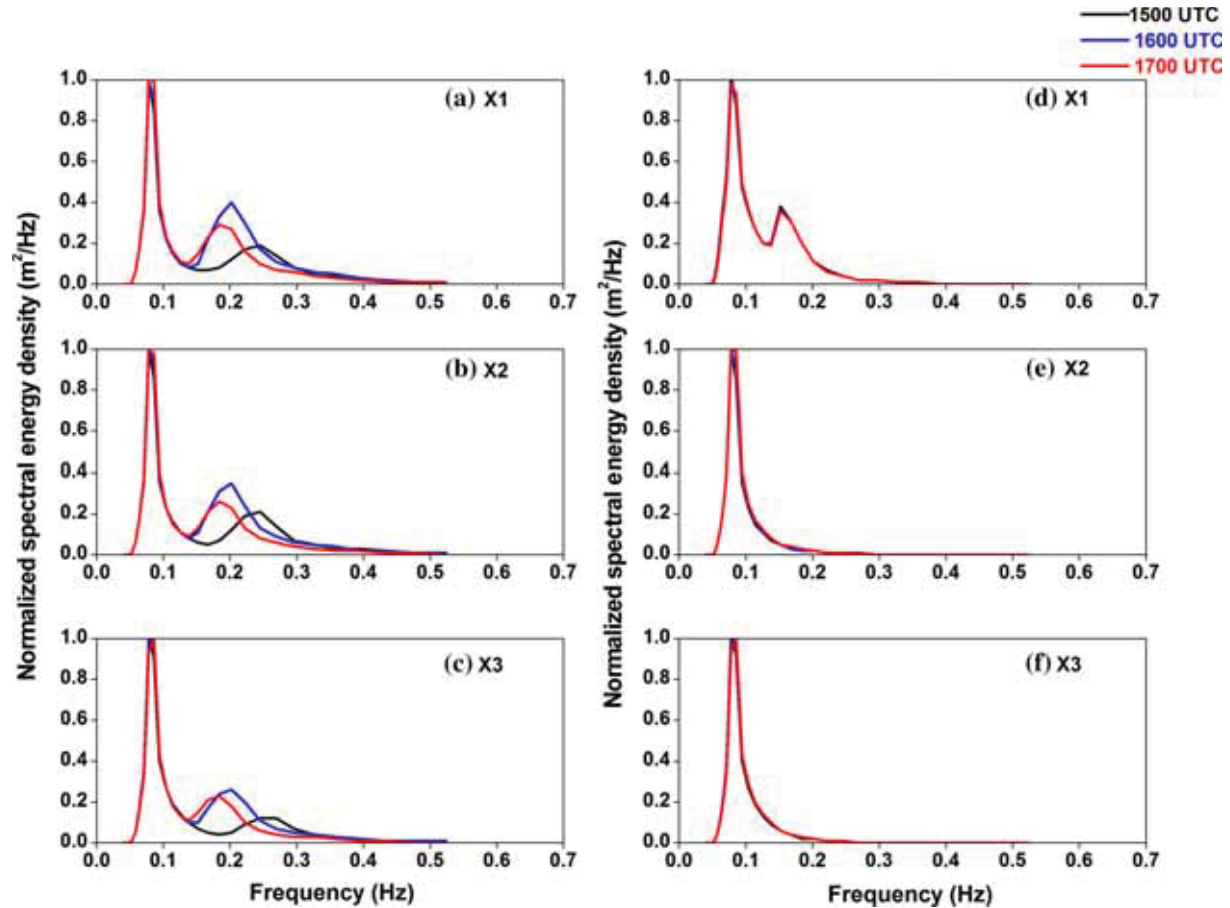

Figure 11. One-dimensional wave spectra at Rameswaram coast on a particular day (2 May 2014). The plots (**a**, **b** and **c**) are obtained from simulations from WRF and plots (**d**, **e** and **f**) are from ECMWF.
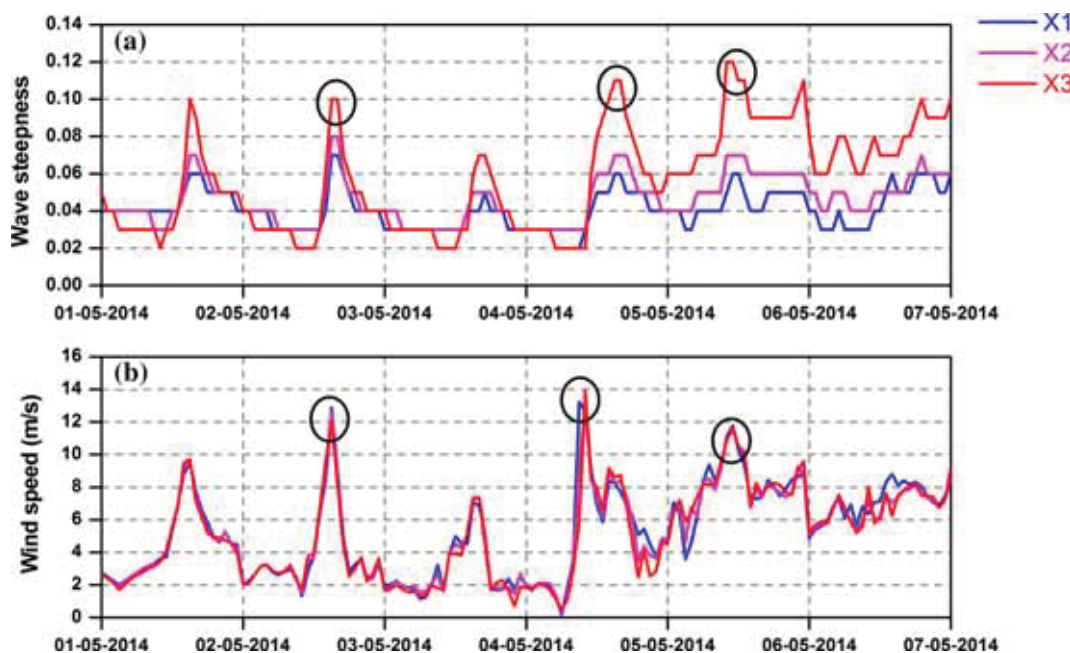
Figure 12. Variation of wave steepness with the wind speed at the Rameswaram coast.

INCOIS has received feedback from the fisherfolk of the Rameswaram region in which they clearly mentioned about the sudden change in the wind speed (~ 11.11 m/s) on 2 May 2014 near Rameswaram and these high winds caused severe damage to fishing boats (minimum of 30–40 boats, furnished based on user feedback). From our study, it is clear that forecasted wind speed (WRF) on 2 May 2014 was 12 m/s (figure 9b), and ASCAT observation shows winds of 12.86 m/s (figure 9c) during this particular day that nearly coincide with visual observations obtained from fisherfolk. These events are resolved by WRF because of high-spatial (3 km) and temporal (1 h) resolution which makes it possible to predict the local features effectively. This once again confirms that the high-resolution meteorological forcing winds are essential to predict the local wind features. The detailed analysis of this event is limited because of the lack of observation data near Rameswaram.

The short duration strong winds might generate steep high waves dangerous for small crafts and hence we analysed the impact on wave using $H_{\max}$ and steepness. The $H_{\max}$ simulated with WRF winds shows a high-wave patch of 3–4 m in the domain on 2 May 2014, whereas the wave simulated with ECMWF could not produce these high waves (figure 10). Due to the unavailability of observation, we have selected three locations (X1, X2 and X3) at a distance of ~ 10, 20 and 30 km from the southern Rameswaram coast from the model simulations of the WRF and ECMWF outputs. A comparison of

$H_{\max}$ from both ECMWF and WRF model simulations is shown in figure 10. The spatial contours show that $H_{\max}$ at X3 was ~ 4 m (figure 10a) whereas ECMWF shows ~ 3 m only (figure 10b). Similarly, $H_{\max}$ at X2 and X1 were in the range of 3.5 and 3 m in WRF simulation whereas ECMWF shows 2.5 and 1.5 m, respectively. It is noticed that $H_{\max}$ (WRF and ECMWF) differ by ~ 1 m at X1, X2 and X3 locations. Furthermore, we made a comparison of normalised spectral energy density at X1, X2 and X3 on a particular day (2 May 2014, 1500–1700 UTC) which is shown in figure 11. Wave spectra from WRF (figure 1a–c) exhibited high-frequency variations (PF>0.2 Hz) whereas spectra from ECMWF have not produced these high-frequency peaks. Furthermore, we have analysed wave steepness during strong wind events near the Rameswaram coast (figure 12a).

It is also seen that the steepness of the waves were increased (i.e., >0.05 at X1 and X2, >0.10 at X3) during the events (figure 12a and b). An increase in wave steepness is marked by a circle in figure 12. According to the study made by Niclasen *et al.* (2010), a wave of 4 m and a steepness of 0.05 are critical limits for small crafts and vessels.

5. Conclusions

This study is an attempt to analyse the importance of a high-resolution wave forecasting system for Tamil Nadu coast during the pre-monsoon period.

Wave fields are simulated using the MIKE21 SW model with two different wind fields, WRF (3 km, 1 h) and ECMWF (27.5 km, 3 h). The simulated wave fields are then used for identifying the local wind and wave features. This study mainly focused on the diurnal variations near Pondicherry coast and the kondalkattu event near Rameswaram.

A comparison of forecast winds (WRF and ECMWF) with AWS and ASCAT and statics clearly shows the reliability of WRF over ECMWF near the coastal areas of India during the pre-monsoon season. Wave spectra comparison, i.e., normalised and frequency-energy spectra, strongly points the requirement of high-resolution winds for the prediction of coastal waves during the pre-monsoon season. This study has proved the importance of fine scale local wind features for Tamil Nadu coast for an accurate wave prediction. It also shows that the Pondicherry coast experiences steep SP waves 80% of time during the pre-monsoon period. The steep waves were well forecasted with WRF winds whereas ECMWF predicted regular low waves which are safe for small crafts throughout the period. The wave forecast with coarse resolution winds are misleading and it proves the importance of high-resolution winds in the wave forecast system.

Furthermore, we tried exploring the impact of short duration strong winds (locally known as kondalkattu) on waves. The strong wind events damaged boats and other coastal properties, the prediction of which was very crucial. Our analysis shows that the high-resolution WRF winds accurately reproduced the sudden variations in the observation winds from ASCAT at Rameswaram. The reason for this sudden variation of wind is the land surface heating during the pre-monsoon season, which causes the formation of low pressure over the Tamil Nadu coast. This pressure difference creates a sudden rise of winds near Rameswaram. Our study clearly points that high-resolution models are required to simulate these events and WRF is able reproduce it to a greater extent. The high-resolution winds certainly predicted the high-frequency waves during the kondalkattu events. The sudden rise in wind speed caused a maximum wave height of 4 m with a steepness of 0.05. Such high wind and wave conditions are dangerous for navigation especially, for small crafts.

This study clearly shows that the importance of an accurate representation of local fine-scale features in the wave forecast for the south-east coast of India during the pre-monsoon for issuing a proper alert or warning mechanism essentially is required for the safe navigation of small crafts. Even though the study was carried out with a small coastal region of India in focus, the conclusions are valid for all the coastal areas around the globe where the fine-scale local features of wind and wave are prominent.

Acknowledgements

References

Abdalla S and Cavaleri L 2002 Effect of wind variability and variable air density on wave modeling; *J. Geophys. Res.* **107** 1–17.

Aboobacker V M, Vethamony P, Sudheesh K and Rupali S P 2009 Spectral characteristics of the nearshore waves off Paradip, India during monsoon and extreme events; *J. Nat. Hazards* **49** 311–323.

Aboobacker V M, Rashmi R, Vethamony P and Menon H B 2011 On the dominance of pre-existing swells over wind seas along the west coast of India; *J. Cont. Shelf Res.* **31** 1701–1712.

Aboobacker V M, Vethamony P, Samiksha S V, Rashmi R and Jyoti K 2013 Wave transformation and attenuation along the west coast of India: Measurements and numerical simulations; *J. Coast. Eng.* **55(1)** 1–21, https://doi.org/10.1142/s0578563413500010.

Aboobacker V M, Seemanth M, Samiksha S V, Sudheesh K, Kerkar J and Vethamony P 2014 Sea breeze-induced wind sea growth in the central west coast of India; *J. Ocean Eng.* **84** 20–28.

Aparna M, Shetye S R, Shankar D, Shenoi S S C, Mehra P and Desai R G P 2005 Estimating the seaward extent of sea breeze from QuikSCAT scatterometry; *J. Geophys. Res. Lett.* **32** 1–4.

Andersson 2013 User guide to ECMWF forecast products; Ver. 1.1, New terminology, ENS initial perturbations.

Anoop T R, Sanil Kumar V, Shanas P R and Glejin J 2015 Surface wave climatology and its variability in the North Indian Ocean based on ERA-Interim reanalysis; *J. Atmos. Ocean. Technol.* **32** 1372–1385.

Balakrishnan Nair T M, Sirisha P, Sandhya K G, Srinivas K, Sanil Kumar V, Sabique L, Arun N, Krishna Prasad B, Rakhi K and Jeyakumar C 2013 Performance of the ocean state forecast system at Indian National Centre for Ocean Information Services; *Curr. Sci.* **105** 175–181.

Barstow S F and Kollstad T 1991 Field trails of directional wave rider; *Proceedings of the First International Offshore and Polar Engineering Conference*, III, pp. 55–63.

Bentamy A and Fillon D C 2012 Gridded surface wind fields from Metop/ASCAT measurements; *Int. J. Remote Sens.* **33** 1729–1754.

Bertotti L, Cavaleri L, Loffredo L and Torrisi L 2013 Nettuno: Analysis of a wind and wave forecast system for the Mediterranean Sea; *J. Mon. Weather Rev.* **141** 3130–3141.

Bidlot J R, Holmes D J, Wittmann P A, Lalbeharry R and Chen H S 2002 Inter-comparison of the performance of operational ocean wave forecasting systems with buoy data; *Weather Forecast.* **17** 287–310.

Bryant M A, Hesser T J and Jensen R E 2016 *Evaluation Statistics Computed for the Wave Information Studies (WIS)*; US Army Corps of Engineers, pp. 1–10.

Cavaleri L 1994 Applications to wave hindcasting and forecasting; Chapter IV; In: *Dynamics and Modeling of Ocean Waves* Cambridge University Press, UK, 532p.

Chawla A, Tolman H L, Gerald V, Spindler D, Spindler T, Alves J H G M, Cao D, Hanson J L and Devaliere E M 2013 A multi grid wave forecasting model: A new paradigm in operational wave forecasting; *J. Weather Forecast.* **28** 1057–1078, https://doi.org/10.1175/WAF-D-12-00007.1.

Das P K 1995 The monsoons. National government publication. India. Directional Wav rider MkIII. Data well-oceanographic instruments; https://www.uniquegroup.com/item/1050/WaveMonitoring/Datawell-Directional-Waverider-Mk3-Buoy.html.

Dinesh Kumar E, Sannasiraj S A, Sundar V and Polnikov V G 2013 Wind-wave characteristics and climate variability in the Indian Ocean region using altimeter data; *J. Mar. Geod.* **36** 303–318.

Glejin J, Sanil Kumar V, Balakrishnan Nair T M and Singh J 2013 Influence of winds on temporally varying short and long period gravity waves in the near shore regions of the eastern Arabian Sea; *J. Ocean Sci.* **9** 343–353.

Golshani A, Nakhaee A, Taebi S, Chegini V and Alaee M J 2005 Wave hindcast study of the Caspian Sea; *J. Mar. Eng.* **1** 19–25.

Goswami B N and Rajagopal E N 2003 Indian Ocean surface winds from NCMRWF analysis as compared to QuickS-CAT and moored buoy winds; *J. Earth Syst. Sci.* **112** 61–77.

Goward Brown A J, Neill S and Lewis M 2013 The influence of wind gustiness on estimating the wave power resource; *Int. J. Mar. Energy* **3–4** 1–10.

Hemer M A, Fan Y, Mori N, Semedo A and Wang X L 2013 Projected changes in wave climate from a multi-model ensemble; *J. Nat. Clim. Change,* 471–476. https://doi.org/10.1038/nclimate1791.

Indira Rani S and Das Gupta M 2013 Oceansat-2 and RAMA buoy winds: A comparison; *J. Earth Syst. Sci.* **122** 1571–1582.

Indira Rani S, Ramachandran R, Bala Subrahamanyam D, Alappattu D P and Kunhikrishnan P K 2010 Characterization of sea/land breeze circulation along the west coast of Indian sub-continent during pre-monsoon season; *J. Atmos. Res.* **95** 367–378.

Jose F, Kobashi F D and Stone G W 2007 Spectral wave transformation over an elongated sand shoal off South-Central Louisiana, U.S.A; *J. Coast. Res.* **50** 757–761.

Kurian N P, Rajith K, Shahul Hameed T S, Sheela Nair L, Ramana Murthy M V, Arjun S and Shamji V R 2009 Wind waves and sediment transport regime off the south-central Kerala coast India; *Nat. Hazards* **49** 325–345.

Michalakes J, Dudhia J, Gill D, Henderson T, Klemp J, Skamarock W and Wang W 2004 *The Weather Research and Forecast Model: Software Architecture and Performance*; https://doi.org/10.1142/9789812701831_0012.

Nayak S, Bhaskaran P K, Venkatesan R and Dasgupta S 2013 Modulation of local wind waves at Kalpakkam from remote forcing effects of Southern Ocean swells; *J. Ocean Eng.* **64** 23–35.

Neetu S, Shetye S and Chandramohan P 2006 Impact of sea breeze on wind-seas off Goa, west coast of India; *J. Earth Syst. Sci.* **115** 229–234.

Niclasen B A, Simonsen K and Magnusson A K 2010 Wave forecasts and small-vessel safety: A review of operational warning parameters; *J. Mar. Struct.* **23** 1–21.

Peixoto J P and Oort A H 1992 *Physics of Climate*; American Institute of Physics, Woodbury, NY.

Powers J G, Klemp J B, Skamarock W C, Davis C A, Dudhia J, Gill D O, Coen J, Gochis D J, Ahmadov R, Peckham S E, Grell G A, Michalakes J, Tahan S, Benjamin S G, Alexander C R, Dimego G J, Wei Wan G, Scwartz C, Romine G S, Liu Z, Snyder C, Chen F, Barlage M J, Yu W and Duda M G 2017 The weather forecasting model overview, system efforts and future directions; *Bull. Am. Meteorol. Soc.* **98** 1717–1737.

Remya P G and Kumar R 2013 Impact of diurnal variation of winds on coastal waves off South East Coast of India; *Int. J. Ocean Clim. Syst.* **4** 171–179.

Remya P G, Kumar R, Basu S and Sarkar A 2012 Wave hindcast experiments in the Indian Ocean using MIKE 21 SW model; *J. Earth Syst. Sci.* **121** 385–392.

Remya P G, Vishnu S, Praveen Kumar S and Balakrishnan Nair T M 2016 Tele connection between the North Indian Ocean high swell events and meteorological conditions over the Southern Indian; *J. Geophys. Res.* **121** 7476–7494.

Sabique L, Annapurnaiah K, Balakrishnan Nair T M and Srinivas K 2012 Contribution of Southern Indian Ocean swells on the wave heights in the Northern Indian Ocean – A modeling study; *J. Ocean Eng.* **43** 113–120.

Sanil Kumar V and Anjali Nair M 2015 Inter-annual variations in wave spectral characteristics at a location off the central west coast of India; *J. Ann. Geophys.* **33** 159–167.

Schiller A, Davidson F, Digiacomo P M and Kirsten W-B 2016 Better informed marine operations and management. Multidisciplinary efforts in ocean forecasting research for socioeconomic benefit; *Bull. Am. Meteorol. Soc.* **97(9)** 1553–1559. https://doi.org/10.1175/BAMS-D-15-00102.1.

Simpson J H, Hyder P, Rippeth T P and Lucas I M 2002 Forced oscillations near the critical latitude for diurnal-inertial resonance; *J. Phys. Oceanogr.* **32** 177–187.

Simpson Mathew, Warrior Hari, Raman Sethu Aswatha-narayana P A, Mohanty U C, Suresh R 2007 Sea-breeze-initiated rainfall over the east coast of India during the Indian southwest monsoon. *J Natural Hazards.* **42**, 401–413. https://doi.org/10.1007/s11069-006-9081-2

Sindhu B, Suresh I, Unnikrishnan A S, Bhatkar N V, Neetu S and Michael G S 2007 Improved bathymetric datasets for the shallow water regions in the Indian Ocean; *J. Earth Syst. Sci.* **116** 261–274.

Sirisha P, Remya P G, Balakrishnan Nair T M and Venkateswara Rao B 2015 Numerical simulation and observation of very severe cyclone generated wave fields in the North Indian Ocean; *J. Earth Syst. Sci.* **24** 1639–1651.

Sirisha P, Sandhya K G, Balakrishnan Nair T M and Venkateswara Rao B 2017 Evaluation of wave forecast in the north Indian Ocean during extreme conditions and winter monsoon; *J. Oper. Oceanogr.* **10** 79–92.

Sivareddy S, Ravichandran M, Sivasankaran Girishkumar M and Siva Rama Prasad K V 2015 Assessing the impact of various wind forcing on INCOIS-GODAS simulated ocean currents in the equatorial Indian Ocean; *J. Ocean Dyn.* **65** 1235–1247.

Skamarock W C, Klemp J B, Dudhia J, Gill D O, Barker D M, Duda M G, Huang X-Y, Wang W and Powers J G 2008 A description of the Advanced Research WRF version. NCAR Tech; National Center for Atmospheric Research. http://opensky.ucar.edu/islandora/object/technotes:500.

Sorensen O R, Kofoed-Hansen H, Rugbjerg M and Sorensen L S 2004 A third-generation spectral wave model using an unstructured finite volume technique; *Proc. Int. Conf. Coast. Eng.* **29** 894–906.

Steven L B, Hesser T J and Jensen R E 2016 Evaluation Statistics Computed for the Wave Information Studies (WIS); In *Proceedings of ERDC/CHL*. CHETN-91.

Tolman H L, Banner M L and Kahitu J M 2013 The NOPP operational wave model improvement project; *J. Ocean Model.* **70** 2–10.

Vethamony P, Sudeesh K, Rupali S, Babu M T, Jayakumar S, Saran A K, Basu S K, Kumar R and Sarkar A 2006 Wave modelling for the north Indian Ocean using MSMR analysed winds; *Int. J. Remote Sens.* **27** 3767–3780.

Vethamony P, Aboobacker V M, Sudheesh K, Babu M T and Ashok Kumar K 2009 Demarcation of inland vessels limit off Mormugao port region, India: A pilot study for the safety of inland vessels using wave modeling; *Nat. Hazards* **49** 411–420.

Vethamony P, Aboobacker V M, Menon H B, Ashok Kumar K and Cavaleri L 2011 Superimposition of wind season pre-existing swells off Goa coast; *J. Mar. Syst.* **87** 47–54.

Vishnu S and Francis P A 2014 Evaluation of high-resolution WRF model simulations of surface wind over the West Coast of India; *J. Atmospheric Ocean. Sci. Lett.* **7**(**5**) 458–463.

Woodcock F and Greenslade D J M 2007 Consensus of numerical model forecasts of significant wave heights; *Weather Forecast.* **22** 792–803.

Corresponding editor: N V Chalapathi Rao